A New Simple Asymmetric Hysteresis Operator and its Application to Inverse Control of Piezoelectric Actuators

Adrien Badel, Jinhao Qiu, and Tetsuaki Nakano

***Abstract*—Piezoelectric actuators (PEAs) are commonly used as micropositioning devices due to their high resolution, high stiffness, and fast frequency response. Because piezoceramic materials are ferroelectric, they fundamentally exhibit hysteresis behavior in their response to an applied electric field. The positioning precision can be significantly reduced due to nonlinear hysteresis effects when PEAs are used in relatively long-range applications. This paper describes a new, precise, and simple asymmetric hysteresis operator dedicated to PEAs. The complex hysteretic transfer characteristic has been considered in a purely phenomenological way, without taking into account the underlying physics. This operator is based on two curves. The first curve corresponds to the main ascending branch and is modeled by the function f_1. The second curve corresponds to the main reversal branch and is modeled by the function g_2. The functions f_1 and g_2 are two very simple hyperbola functions with only three parameters. Particular ascending and reversal branches are deduced from appropriate translations of f_1 and g_2. The efficiency and precision of the proposed approach is demonstrated, in practice, by a real-time inverse feed-forward controller for piezoelectric actuators. Advantages and drawbacks of the proposed approach compared with classical hysteresis operators are discussed.**

I. Introduction

Piezoelectric actuators (PEAs) are commercially available devices widely used for micropositioning operations in the range of 10 pm to 100 μm. For high-accuracy positioning and tracking systems, the piezoactuated positioning mechanism should be equipped with a controller. Modern controller designs are based on a model of the system to be controlled.

The positioning precision is mainly affected by the nonlinear hysteresis effect exhibited in ferroelectric materials, especially when PEAs are used in relatively long-range applications. A large number of controllers have then been developed focusing on hysteresis compensation. Most of these methods use an inverse model of hysteresis in the controller. This inverse model is often based on a Preisach model of hysteresis [1]–[4], a Generalized Maxwell Slip (GMS) model of hysteresis [5], or a Prandt Ishlinkii operator [6].

The GMS model of hysteresis, precisely described in [7], as well as the Prandt Ishlinkii model are quite simple and easy to implement in a real-time controller. Their main drawback is that only centrally symmetric hysteresis loops can be modeled, whereas in many PEAs, hysteresis loops exhibited between the voltage and the displacement are slightly asymmetric. The Preisach model of hysteresis is a very general model of hysteresis that can model asymmetric hysteretic loops [8]. It has been widely used to design feed-forward controllers. Its main drawbacks are that it has a stepped response and that it requires a large number of parameters whose identification procedure is heavy and relatively complicated.

A modified Prandt-Ishlinkii operator has been recently proposed, where a nonsymmetrical nonlinearity is added to the classical Prandt Ishlinkii operator, allowing modeling of asymmetric hysteresis loops [9]. This approach is a simpler alternative to the Preisach operator.

In this paper, a new, very simple inverse hysteresis operator dedicated to PEA control is presented. The proposed operator can model asymmetric hysteresis loops and is much simpler than the Preisach model of hysteresis and even simpler than the modified Prandt-Ishlinkii operator. It is defined by two hyperbola functions, each described by only three parameters. These parameters can be very easily determined using one experimental displacement-voltage hysteresis loop. This operator is not as complete as the Preisach or the modified Prandt-Ishlinkii operator, but it is applicable in most PEA operating conditions.

The feed-forward control principle is described in Section II. The proposed hysteresis operator is then detailed in Section III, and the wiping-out and the congruency property are discussed. Comparisons between measurements and simulation using both the proposed and the Preisach operator are presented in Section IV. In Section V, the proposed approach is used in a real-time feed-forward controller. Experimental results show that the proposed operator precisely models the hysteresis loops of the controlled PEA transfer characteristic and that a precise tracking control is possible without any displacement sensor.

II. Objectives

The goal of this study is to develop an inverse hysteresis operator used as a feed-forward controller for the

Manuscript received April 25, 2007; accepted January 16, 2007.

A. Badel is with the Institute of Fluid Science, Tohoku University, Aoba-ku, Sendai-Shi, Japan.

J. Qiu is with the College of Aerospace Engineering, Nanjing University of Aeronautics and Astronautics, Nanjing, China (e-mail: qiu@nuaa.edu.cn).

T. Nakano is with the Honda Automobile R&D Center, Tochigi, Japan.

Digital Object Identifier 10.1109/TUFFC.2008.761

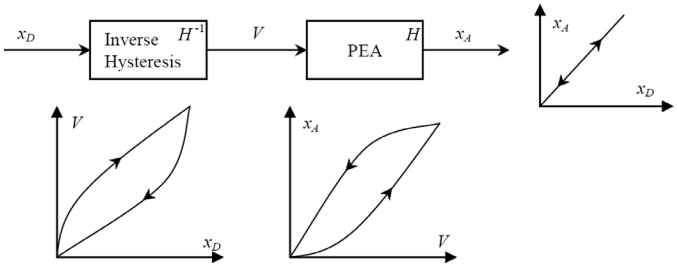

Fig. 1. Inverse control principle.

TABLE I
PIEZOELECTRIC ACTUATOR MAIN CHARACTERISTICS.

Type	NEC/TOKIN (AE1010D16)
Dimensions	$10 \times 10 \times 20$ mm^3
Capacitance	5.4 μF
Curie Temperature	180°C
Displacement @ 100 V	12.3 μm
Force @ 100 V	3500 N
Maximum Voltage	120 V
Young's Modulus	4.4×10^{10} N/m^2
First Resonance Frequency	3 kHz

compensation of hysteresis in the transfer characteristic of a piezoelectric actuator. This controller principle is shown in Fig. 1, where x_D is the desired displacement, V is the driving voltage, and x_A is the measured displacement. Let H be the hysteresis operator corresponding to the displacement versus driving voltage characteristic. If the feed-forward controller corresponds exactly to the inverse hysteresis operator H^{-1}, then the measured displacement is equal to the desired displacement. The actuator used in this study is a multilayered PEA from NEC/TOKIN. Its main characteristics are summarized in Table I. As any PEA, this actuator exhibits hysteresis behavior in its mechanical response to an applied driving voltage. Fig. 2(a) shows a major hysteresis loop between the driving voltage and the displacement (elongation) of the PEA. The driving voltage is plotted versus the displacement; the hysteresis loops corresponds then to H^{-1}. In this paper, a so-called "major loop" corresponds to a zero → maximal voltage/displacement → zero profile. To highlight the hysteresis effect, the hysteretic characteristic of the PEA can be decomposed as the summation of a linear and a hysteretic response. This is shown in (1), where α is a proportional coefficient and H_E is a new emphasized hysteresis operator. Fig. 2(b) shows the hysteresis loop between the displacement and V_H, when α is equal to 6 V/μm. The hysteresis effect appears in a clearer manner in this plot, and it is shown that the exhibited loop does not have a central symmetry. The value of α is arbitrary. It was chosen so that the derivative of the major reversal branch reaches zero around the origin. Large and clear hysteresis loops are then exhibited.

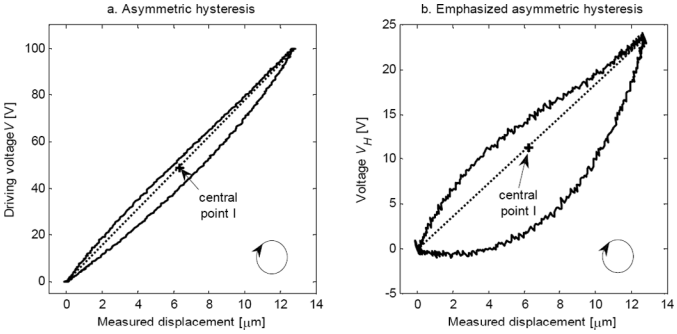

Fig. 2. Experimental asymmetric hysteresis loops.

$$\begin{cases} V = \alpha x + V_H \\ V_H = H_E(x) \end{cases} . \tag{1}$$

Because of this asymmetry, the GMS operator cannot be applied to model voltage versus displacement transfer function. The Preisach model of hysteresis can be used. In practice, the classical Preisach model consists of a weighted combination of elementary relay hysteresis elements, and then it exhibits a stepped response. More precisely, if $n(n+1)/2$ elements are used, then a major ascending branch exhibits n steps. The main drawback of this approach is that a huge number of elements have to be used to get a precise modeling and that the procedure to get the weights associated with each element is very heavy. The goal of the proposed approach is to provide a simple hysteresis operator exhibiting asymmetric loops. Control performances using this operator as a feed-forward controller are not better than performances using a Preisach type operator, but the identification procedure as well as the implementation and memory requirements are much lighter.

III. Proposed Hysteresis Operator Theory

A. Basis

Hysteresis loops using the studied PEA are not symmetric. This can be easily seen on Fig. 3(a), where the black loop corresponds to the experimental asymmetric major hysteresis loop, and the gray curve corresponds to the ascending branch if the hysteresis behavior were symmetric around the central point I.

The proposed approach is based on two curves. The first curve corresponds to the major ascending branch and is modeled by the function f_1. The second curve corresponds to the major ascending branch if the hysteresis loop were symmetric around I and is modeled by the function f_2. Both curves are shown in Fig. 3(b). The functions f_1 and f_2 are two very simple functions with only three parameters, as shown in (2). These parameters can easily be determined using classical fitting tools, starting from the major ascending branch (for f_1) and the symmetric of the major reversal branch around I (for f_2). Identified parameters for the studied PEA are given in Table II.

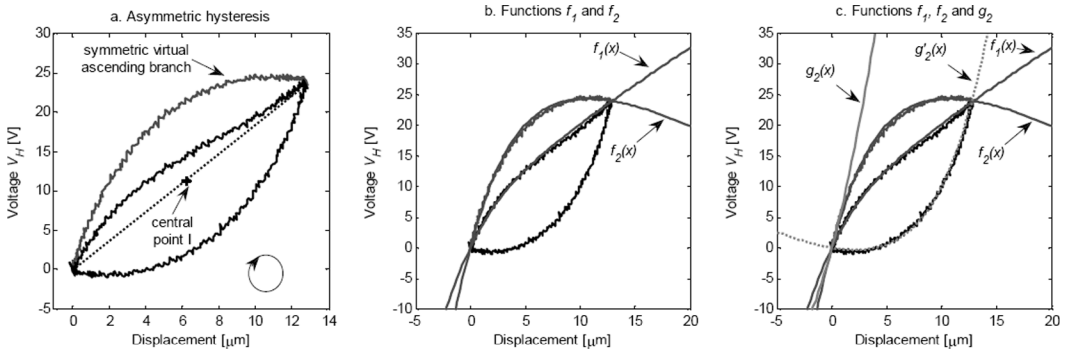

Fig. 3. Constitutive equations of the asymmetric hysteresis operator.

TABLE II
PARAMETERS OF THE HYSTERESIS OPERATOR.

a_1 (V)	10.1
b_1 (μm)	4.13
c_1 (V/μm)	3.50
a_2 (V)	51.1
b_2 (μm)	6.49
c_2 (V/μm)	6.7

$$\begin{cases} f_1(x) = a_1\left(1-\sqrt{1+\dfrac{x^2}{b_1^2}}\right)+c_1x \\ \\ f_2(x) = a_2\left(1-\sqrt{1+\dfrac{x^2}{b_2^2}}\right)+c_2x \end{cases}. \quad (2)$$

Functions f_1 and f_2 are the two constitutive equations of the hysteresis operator. In this model, all ascending branches are determined using a particular translation of f_1. Function f_1 is then called the "general ascending function." The "general reversal function" is g_2, given by (3), which is the symmetric function of f_2 around the origin. All reversal branches are determined using particular translation of g_2. For example, the reversal branch in Fig. 3(c) is modeled by g_2' which is a particular translation of g_2. The translation mechanisms are described in the next section.

$$g_2(x) = -f_2(-x) = -a_2\left(1-\sqrt{1+\frac{x^2}{b_2^2}}\right)+c_2x. \quad (3)$$

A geometrical analysis of functions f_1 and f_2 is given in Fig. 4. Functions f_1 and f_2 are the summation of a line equation and a hyperbola equation. The slope of the line is c (respectively, c_1 and c_2) and the hyperbola equation is defined by the classical parameters a and b (respectively, a_1, b_1, and $a_2\,b_2$), as shown in Fig. 4(a). Functions f_1 and f_2 are also hyperbolas, whose asymptotes are described in Fig. 4(b). As previously said, parameters of f_1 and f_2 can be determined using fitting tools. The parameters can also be calculated using the slopes of the asymptotes and their crossing point on the y-axis.

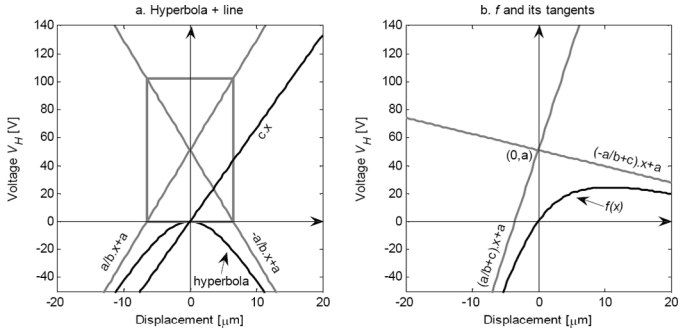

Fig. 4. Constitutive equations geometrical analysis.

B. Translation Mechanisms

The postulate of the proposed approach is that any ascending branch is a particular translation of the general ascending branch associated with the function f_1 and that any reversal branch is a particular translation of the general reversal branch associated with the function g_2.

Ascending and reversal branches are switched each time the input of the hysteresis operator (i.e., the displacement) reaches an extremum. When a minimum of the displacement occurs, the hysteresis operator switches from a reversal branch to an ascending branch, and conversely, when a maximum of the displacement occurs, the hysteresis operator switches from an ascending branch to a reversal branch.

A particular ascending branch passes through its starting point (x_m, V_m), which corresponds to a minimum of the displacement, and through the point (x_M, V_M), corresponding to the last maximum of the displacement, which was reached before the displacement started decreasing to x_m. The particular ascending branch is then the translation of f_1 that passes through (x_m, V_m) and (x_M, V_M). The translated curve is given by (4), where (x_T, V_T) is the coordinate of the translation vector. Variables x_T and V_T can be determined solving the set of (5).

$$V = f_1(x-x_T)+V_T \quad (4)$$

$$\begin{cases} V_m = f_1(x_m-x_T)+V_T \\ V_M = f_1(x_M-x_T)+V_T \end{cases}. \quad (5)$$

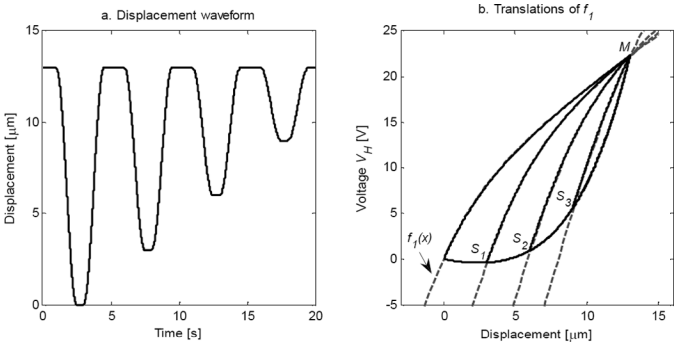

Fig. 5. Ascending branches—Translations of f_1.

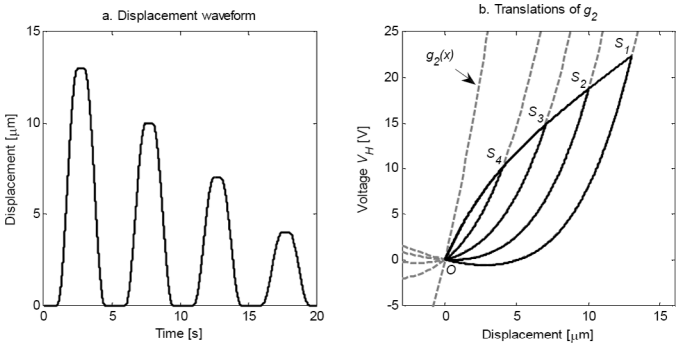

Fig. 6. Reversal branches—Translations of g_2.

Eq. (5) leads to the equation of the translated curve (6), where the only unknown parameter is x_T, which can be determined solving (7).

$$V = f_1(x - x_T) - f_1(x_M - x_T) + V_M, \tag{6}$$

$$f_1(x_M - x_T) - f_1(x_m - x_T) = V_M - V_m. \tag{7}$$

This procedure is illustrated in Fig. 5. The input displacement is given in Fig. 5(a). The corresponding hysteresis loops as well as the function f_1 and its translations are given in Fig. 5(b). In this simple case, the last maximum (x_M, V_M) is always the global maximum M. The ascending branches' starting points (x_m, V_m) are points S_1, S_2, and S_3, respectively. Results presented in this figure have been obtained using a simulink simulation. Implementation of the algorithm will be detailed in Section III-E.

In a way similar to ascending branches, a particular reversal branch is determined by its starting point (x_M, V_M) which corresponds to a maximum of the displacement, and the point (x_m, V_m) corresponding to the last minimum of the displacement, which was reached before the displacement started increasing to x_M. The particular reversal curve is the translation of g_2 that passes through (x_M, V_M) and (x_m, V_m). The equation of the translated curve is given by (8), where only x_T is unknown and can be determined solving (9).

$$V = g_2(x - x_T) - g_2(x_m - x_T) + V_m, \tag{8}$$

$$g_2(x_M - x_T) - g_2(x_m - x_T) = V_M - V_m. \tag{9}$$

This procedure is illustrated in Fig. 6. The input displacement is given in Fig. 6(a). The corresponding hysteresis loops as well as the function g_2 and its translations are given in Fig. 6(b). In this simple case, the last minimum (x_m, V_m) is always the origin O. The ascending branches starting points (x_M, V_M) are points S_1, S_2, S_3, and S_4, respectively.

C. Wiping-Out Property

The wiping-out property refers to the constraint that the output be affected only by the current input and the alternating series of previous dominant input extrema, the effect of all other inputs being wiped out. A dominant maximum is one that is greater than any subsequent maximum, while a dominant minimum is one that is less than any subsequent minimum.

Let us see how the wiping-out property is included in the proposed operator. Let (10) be the alternating series of previous dominant input extrema. This means that any maximum of this series is larger than all subsequent maxima, and that any minimum is smaller than all subsequent minima, as shown in (11). The series of the corresponding voltages is given by (12). In this case, we consider that the last extremum is a maximum (x_M^n).

$$x_M^n, x_m^n, x_M^{n-1}, x_m^{n-1}, x_M^{n-2}, x_m^{n-2}, \ldots, x_M^1, x_m^1, \tag{10}$$

$$\begin{cases} x_m^n > x_m^{n-1} > x_m^{n-2} > \cdots > x_m^1 \\ x_M^n < x_M^{n-1} < x_M^{n-2} < \cdots < x_M^1 \end{cases}, \tag{11}$$

$$V_M^n, V_m^n, V_M^{n-1}, V_m^{n-1}, V_M^{n-2}, V_m^{n-2}, \ldots, V_M^1, V_m^1. \tag{12}$$

Starting from x_M^n, the reversal branch is the translation of g_2 that passes through (x_M^n, V_M^n) and the previous minimum (x_m^n, V_m^n). If the displacement decreases under x_m^n, then x_m^n and x_M^n are wiped out, the reversal branch is changed and becomes the translation of g_2 that passes through the two previous dominant extrema, which are (x_M^{n-1}, V_M^{n-1}) and (x_m^{n-1}, V_m^{n-1}). This branch naturally passes also through (x_m^n, V_m^n).

The procedure is the same for the ascending branches. Let us suppose that the displacement starts increasing just after it decreased under x_m^n. A new minimum is created, called x_m^n, because the previous x_m^n has been wiped out. If the displacement rises above x_M^{n-1}, then x_M^{n-1} and x_m^n are wiped out and the ascending branch becomes the translation of g_2 that passes through (x_m^{n-1}, V_m^{n-1}) and (x_M^{n-2}, V_M^{n-2}). This wiping-out sequence is illustrated in Fig. 7, with $n = 3$. Fig. 7(a) shows the input displacement waveform and the wiping-out effect. The corresponding complex hysteresis loops, as well as the associated translation of f_1 and g_2 are plotted on Fig. 7(b). After the displacement reaches point A, it becomes smaller than the last dominant minimum x_m^3; x_M^3 and x_m^3 are then wiped out. A new x_m^3 is created at point B, where the displacement reaches a minimum. At point C, the displacement becomes

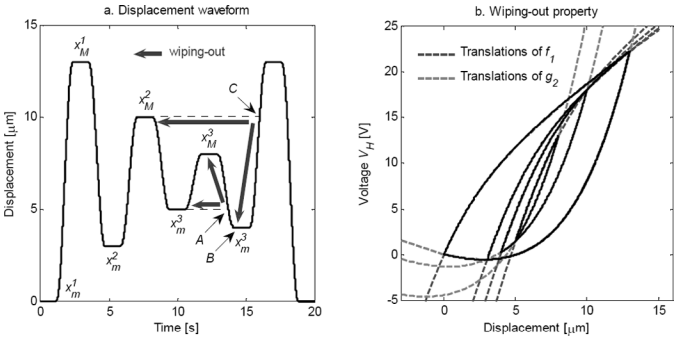

Fig. 7. Ascending and reversal branches—Wiping-out property.

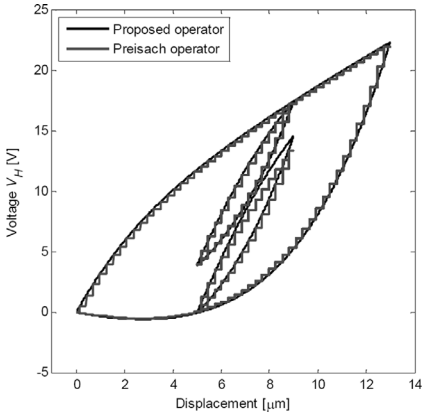

Fig. 8. Congruent and noncongruent minor loops.

larger than the last dominant maximum x_M^2. The new x_m^3 and x_M^2 are then wiped out.

D. Congruency Property

A minor loop is defined as a loop described when the input varies from x_a to x_b and then goes back to x_a without any intermediate extremum. The congruency property refers to the fact that the shape and size of a minor loop is only a function of its input range $[x_a, x_b]$ and is independent of the input history. The congruency property is fulfilled by most of the classical hysteresis operators, such as the Preisach and the GMS operator, but not by the proposed operator. Fig. 8 shows two minor loops with the same input range using the Preisach operator and using the proposed approach.

The Preisach model is composed of 1275 single relays. Its major ascending branch exhibits then 50 steps. The 1275 coefficients of the Preisach operator have been determined so that the major ascending branch and all reversal branches starting from it and going back to zero are similar for both the Preisach and the proposed operators. The identification procedure is not described here, but can be found in [10].

It is shown in Fig. 8 that the Preisach operator complies with the congruency property, contrary to the proposed approach. However, it is also shown that minor loops from both operators are very close. It will be shown in Section IV that it is difficult to distinguish which operator corresponds best to experimental measurements. Both of them give satisfactory predictions.

E. Algorithm Implementation

In the Simulink environment, the hysteresis operator is implemented as an S-function written in the C language. This function has seven parameters. The six first parameters are a_1, b_1, c_1, a_2, b_2, and c_2. The seventh parameter is the "memory depth," which corresponds to the number n of dominant minima and maxima that can be stored by the S-function in addition to the latest previous extremum.

Fig. 9 shows simulation results for the same input profiles but for different values of the memory depth n. The input profile is given by (13), where 0, x_m^2, x_m^3, and x_m^4 are dominant minima, and x_M^1, x_M^2, x_M^3, and x_M^4 are dominant maxima.

$$\{0 \to x_M^1 \to x_m^2 \to x_M^2 \to x_m^3 \to x_M^3 \to x_m^4 \to x_M^4 \to 0\}. \tag{13}$$

In Fig. 9(a), n is set to zero, which means that only the latest previous extrema is stored. After reaching the maximum x_M^4, the reversal branch is calculated as the translation of g_2 that goes through the current position (x_M^4, V_M^4) and the previous minimum (x_m^4, V_m^4). However, the wiping-out property cannot be fulfilled when the displacement decreases under x_m^4, because the dominant maximum (x_M^3, V_M^3) has not been stored. The reversal branch is unchanged. It is however switched to the major reversal branch after their crossing point. When n is zero, the proposed operator does not comply with the wiping-out property. The fact that the major ascending and reversal branches cannot be crossed over is, however, taken into account.

In Fig. 9(b), n is set to one, which means that the three latest dominant extrema are stored. In this case, the wiping-out property is fulfilled after the displacement decreases under x_m^4, and the reversal branch is changed to the translation of g_2 that goes through the previous dominant maximum (x_M^3, V_M^3) and the previous dominant minimum (x_m^3, V_m^3). For faster computation, the translation vector is not calculated again because it is the same as the one calculated previously for the reversal branch linking (x_M^3, V_M^3) and (x_m^4, V_m^4). In practice, the translation vector coordinates along the x-axis (x_T) are stored in the same way as the dominant extrema coordinates. It is then possible to directly use (6) and (8). However, the wiping-out property cannot be fulfilled when the displacement decreases under x_m^3, because the dominant maximum (x_M^3, V_M^2) has not been stored. The reversal branch is then switched to the major reversal branch at their crossing point.

In Fig. 9(c), n is set to 2 and then the five latest dominant extrema are stored. In this case, the wiping-out property is fully fulfilled. After the displacement decreases under x_m^3, the reversal branch is switched to the translation of g_2 that goes through (x_M^2, V_M^2) and (x_m^2, V_m^2). After x_m^2, it is switched to the major reversal branch.

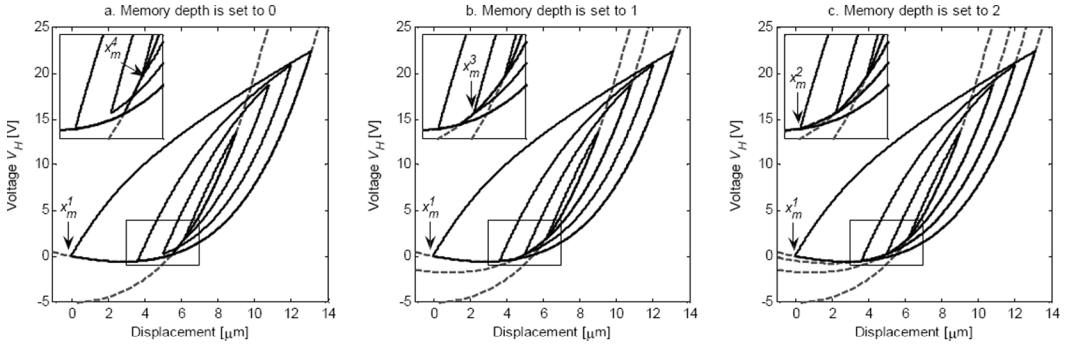

Fig. 9. Wiping-out property, influence of the memory depth.

In most applications, a memory depth equal to three or four is large enough to take the wiping-out property into account correctly. The proposed approach has then very low memory requirements compared with classical hysteresis operators such as the Preisach model. In the case of the Preisach model with a fifty-step ascending branch, the dedicated memory at least corresponds to the 1275 Preisach coefficients plus the 1275 states of the relays. In the case of the proposed approach, only $14+6(n+1)$ variables are stored. Those variables corresponds to the $2n+1$ dominant extrema and related translation vectors, to the seven parameters of the S-function, and to other additional data such as the value of the input and output at the previous sample time.

The required computation time for the proposed operator is extremely low, except when a minimum or maximum occurs. In this case, (7) or (9) has to be solved during one sample time. For now, those equations are solved using a dichotomy algorithm that requires about twenty iterations to get a 0.01% precision. The minimum suitable sample time for the proposed operator implemented in a real-time DSP (DS1103 dSpace board) is about 20 μs, but speed performances may increase using a more efficient solving algorithm.

IV. Simulations and Measurements Comparison

In this section, a comparison of experimental measurements and simulations using both the Preisach and the proposed operators is presented. As noted previously, the coefficients of the Preisach model are calculated so that the major ascending branch and all reversal branches starting from it and going back to zero are similar for both operators. This can be seen in Fig. 10, which exhibits hysteresis loops for different reversal branches. Hysteresis loops simulated by both operators are identical, except the fact that the Preisach operator has a stepped response. Experimental results correspond to the driving voltage profile given by (14). The voltage V_H, defined in (1), is plotted versus the measured displacement x. As explained in Section II, V_H is used instead of the driving voltage V itself to highlight the hysteresis effect. The value of α is still 6 V/μm. As mentioned above, it is an arbitrary value chosen to give clear and large hysteresis loops.

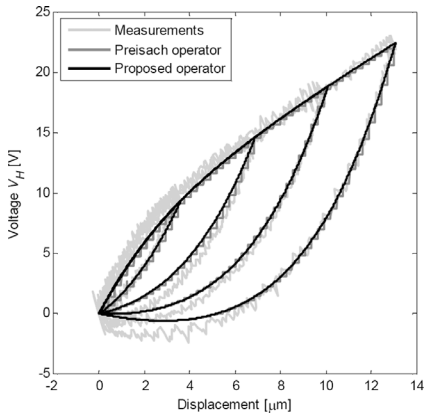

Fig. 10. Comparison of measurements and simulations for different reversal branches.

$$\{0 \rightarrow 100 \rightarrow 0 \rightarrow 77 \rightarrow 0 \rightarrow 54 \rightarrow 0 \rightarrow 31 \rightarrow 0\}\ V. \tag{14}$$

A very good agreement is exhibited between simulations and measurements. Light discrepancies can be seen on the reversal branches when the displacement tends to zero. This is due to the creep effect. When the driving voltage V reaches 0, the measured displacement x is still slightly positive, which implies that $V_H = V - \alpha x$ is slightly negative.

Fig. 11 shows the case of different ascending branches. In this case, simulations using the proposed operator and the Preisach model are slightly different. Experimental results correspond to the driving voltage profile given by (15).

$$\{0 \rightarrow 100 \rightarrow 23 \rightarrow 100 \rightarrow 47 \rightarrow 100 \rightarrow 70 \rightarrow 100 \rightarrow 0\}\ V. \tag{15}$$

Due to the combined effect of creep and measurement imprecision, it is difficult to distinguish which operator gives the best predictions. Both of them satisfactorily model the hysteresis loops.

Minor loops are exhibited in Fig. 12. The corresponding driving voltage profile is given by (16). The conclusion previously drawn also can be drawn here: The proposed approach and the Preisach simulations are slightly different, but both of them are very close from the experimental results.

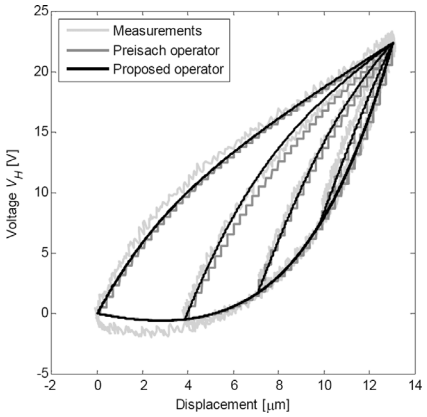

Fig. 11. Comparison of measurements and simulations for different ascending branches.

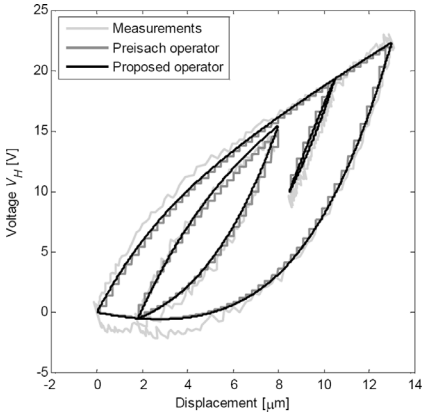

Fig. 12. Comparison of measurements and simulations when minor loops are exhibited.

$$\{0 \rightarrow 80 \rightarrow 60 \rightarrow 100 \rightarrow 10 \rightarrow 60 \rightarrow 0\}\ V. \qquad (16)$$

Of course, the Preisach operator is a much more general model than the proposed one, which can only model hysteresis loops with hyperbola-shaped branches. Piezoelectric actuators, however, exhibit this kind of simple hysteresis loops, and then, due to its simplicity and lightness, the proposed approach offers a good alternative to the Preisach operator.

V. Feedforward Control of an Actuator

In this section, the proposed hysteresis operator is used as a feed-forward real-time controller for the studied PEA. The controller architecture is given by Fig. 13, where x_D is the desired displacement and V is the driving voltage. It is implemented using dSpace hardware hosted by a PC computer. Using the Matlab Real Time Workshop (The MathWorks, Natick, MA), the controller designed and simulated in Simulink is compiled, downloaded, and run in the dSpace hardware. Real-time tracking control is presented for three different desired displacement profiles.

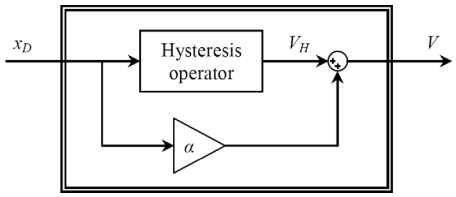

Fig. 13. Feed-forward controller implemented in the Simulink-dSpace environment.

The proposed operator models the hysteresis behavior of the PEA transfer characteristic. Other phenomena may influence the transfer characteristic, such as resistive losses, dielectric losses, mechanical viscous losses, or mechanical oscillations due to the resonances frequencies of the PEA [11]. All these phenomena are negligible at low operating speed. The aim of this study is to develop a simple model of hysteresis, that is why the chosen desired displacement profiles are very low speed compared with the first resonance frequency of the PEA. For high operating speed, the proposed approach could be combined with a PID feedback controller, or additional mechanical and electrical behaviors could be included in the inverse model.

In Fig. 14, only the major ascending branch and different reversal branches of the hysteresis are followed. Fig. 14(a) shows the desired and measured displacement waveforms. Fig. 14(b) shows the measured displacement versus the desired one. Both Fig. 14(a) and (b) show that the expected displacement is almost exactly equal the desired one. Fig. 14(c) shows the voltage V_H versus the desired displacement. This plot corresponds to the hysteresis operator transfer function, that is, the theoretical inverse transfer function of the PEA.

In Fig. 15, only the major reversal branch and different ascending branches of the hysteresis are followed. Plots a, b, and c are similar to the ones presented in the previous figure, and the same conclusion can be drawn: The measured displacement follows precisely the desired one.

A more complex desired displacement is used in Fig. 16. In this case, different ascending and reversal branches are followed and minor loops are described. Even in this case, the proposed feed-forward controller exhibits very good performances.

The proposed hysteresis operator, used as a feed-forward controller, allows a very simple and precise positioning control. The maximal error is about 0.2 μm, and the error is generally lower than 0.1 μm.

VI. Conclusion

A new very simple hysteresis operator was proposed, based on two hyperbola functions. Unlike the General Maxwell Slip model, it can model asymmetric hysteresis loops. This operator is not as complete as the Preisach operator, because only hyperbola-shaped hysteresis can be modeled, but it is sufficient for the majority of PEA ap-

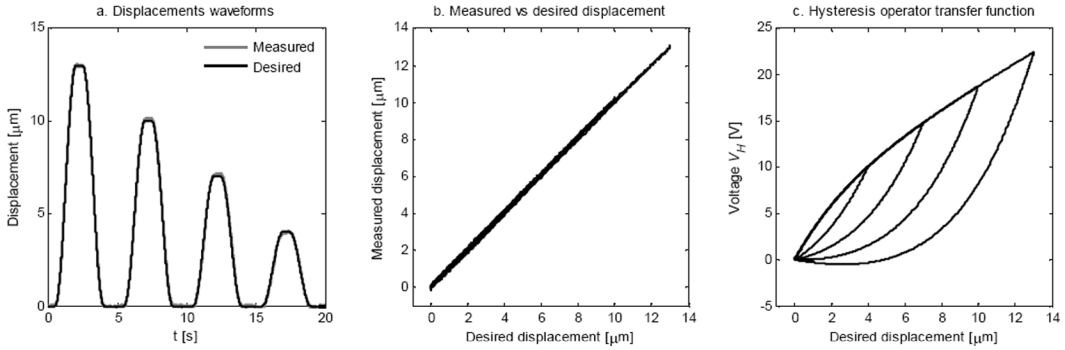

Fig. 14. Tracking control for different reversal branches.

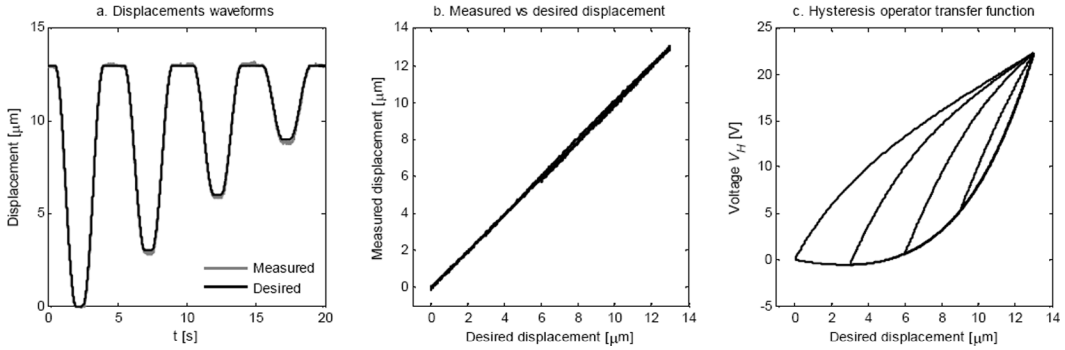

Fig. 15. Tracking control for different ascending branches.

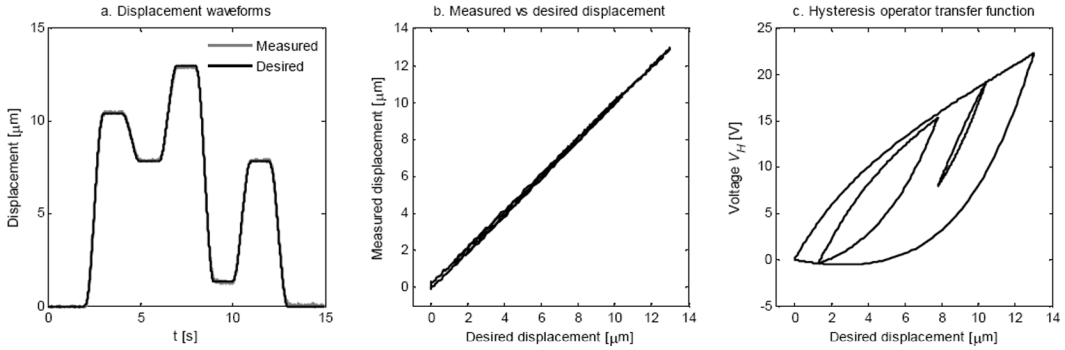

Fig. 16. Tracking control for different ascending and reversal branches.

plications. Whereas the Preisach operator requires a large number of parameters with a complex identification procedure to get precise modeling, the proposed approach only requires six parameters that can be very easily determined. When applicable, the proposed approach may then be efficiently used instead of other more complex hysteresis operators.

The proposed operator was shown to precisely model the hysteresis transfer characteristic of the studied PEA. Moreover, used as a feed-forward controller, it allows a very precise positioning control of the PEA, without using a displacement sensor.

Current work also aims at decreasing the computational time required to calculate the translation vector of the next branch when a minimum or a maximum occurs. For now, a dichotomy algorithm is used to solve (7) and (9). This solving algorithm may be improved. Moreover, the proof of the existence and uniqueness of the solutions of these equations has also to be demonstrated.

References

[1] A. Cavallo, C. Natale, S. Pirozzi, and C. Visone, "Effects of hysteresis compensation in feedback control systems," *IEEE Trans. Magn.*, vol. 39, pp. 1389–1392, 2003.

[2] P. Ge and M. Jouaneh, "Tracking control of a piezoceramic actuator," *IEEE Trans. Contr. Syst. Technol.*, vol. 4, pp. 209–216, 1996.

[3] B. K. Nguyen and K. A. Kyoung, "Hysteresis compensation in SMA actuators through numerical inverse Preisach model implementation," presented at ICCAS, KINTEX, Gyeonggi-Do, Korea, 2005.

[4] G. Song, J. Zhao, X. Zhou, and J. A. De Abreu-Garcia, "Tracking control of a piezoceramic actuator with hysteresis compensation using inverse Preisach model," *IEEE/ASME Trans. Mechatronics*, vol. 10, pp. 198–209, 2005.
[5] P. Mayhan, K. Srinivasan, S. Watechagit, and G. Washington, "Dynamic modeling and controller design for a piezoelectric actuation system used for machine tool control," *J. Intell. Mater. Syst. Struct.*, vol. 11, pp. 771–780, 2000.
[6] K. Kuhnen and H. Janocha, "Adaptive inverse control of piezoelectric actuators with hysteresis operators," presented at European Control Conf., ECC'99, Karlsruhe, Germany, 1999.
[7] M. Goldfarb and N. Celanovic, "Modeling piezoelectric stack actuators for control of micromanipulation," *IEEE Contr. Syst. Mag.*, vol. 17, pp. 69–79, 1997.
[8] D. Hughes and J. T. Wen, "Preisach modeling of piezoceramic and shape memory alloy hysteresis," in *Proc. 4th IEEE Conf. Control Applications*, 1995, pp. 1086–1091.
[9] K. Kuhnen, "Modeling, identification and compensation of complex hysteretic nonlinearities: A modified Prandt-Ishlinkii approach," *Eur. J. Control*, vol. 9, pp. 407–418, 2003.
[10] P. Ge and M. Jouaneh, "Modeling hysteresis in piezoceramic actuators," *Precis. Eng.*, vol. 17, pp. 211–221, 1995.
[11] H. J. M. T. S. Adriaens, W. L. De Koning, and R. Banning, "Modeling piezoelectric actuators," *IEEE/ASME Trans. Mechatronics*, vol. 5, pp. 331–341, 2000.

Jinhao Qiu received the Bachelor's and Master's degrees in mechanical engineering from Nanjing University of Aeronautics and Astronautics, China, in 1983 and 1986, respectively, the Ph.D. degree in mechanical engineering from Tohoku University, Japan, in 1996. He was a research associate from 1986 to 1989 and lecturer 1990 to 1991 at Department of Mechanical Engineering, Nanjing University of Aeronautics and Astronautics. He was a faculty member at the Institute of Fluid Science, Tohoku University, from 1992 to 2006, where he was a research associate from 1992 to 1998, an assistant professor 1998 to 2000, an associate professor from 2000 to 2004 and a professor from 2004 to 2006. Since March, 2006, he has been a professor at the Nanjing University of Aeronautics and Astronautics. His main research interest is smart materials and structural systems, including development of piezoelectric materials and devices, vibration and noise control, and active flow control for aerospace applications.

He has published 87 journal papers, 9 review papers, and more than 120 conference papers. He has also received 5 awards, including The 2002 Annual Dynamics, Measurement and Control Awards for Pioneering Achievements in the research of smart materials and structural systems from The Japan Society of Mechanical Engineers.

Adrien Badel was born in France in 1979. He graduated from Institut National des Sciences Appliquées de Lyon (INSA), Lyon, France, in electrical engineering in 2002 (M.S. degree). He prepared his Ph.D. at the Electrical Engineering and Ferroelectricity Laboratory of INSA Lyon, France. He received his Ph.D. degree in 2005 for his work on vibration control and energy harvesting. From November 2005 to November 2007, he was a JSPS (Japanese Society for the Promotion of Science) postdoctoral fellow at the Institute of Fluid Science of Tohoku University, Sendai, Japan. He is now an assistant professor at the Laboratory of Systems and Materials for Mechatronics from the Savoie University, Annecy, France. His research interests include energy harvesting, vibration damping, and piezoelectric actuators modeling and control.

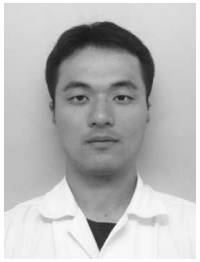

Tetsuaki Nakano was born in Japan in 1978. He received the B.S. and M.S. degrees in Electrical Engineering from Waseda University in 2003. He is now working at Honda R&D Co., Ltd., Automobile R&D Center. His current activities are electrical device control and electric system development for automobiles.